

FEEDBACK FROM CENTRAL BLACK HOLES IN ELLIPTICAL GALAXIES: TWO-DIMENSIONAL MODELS COMPARED TO ONE-DIMENSIONAL MODELS

GREGORY S. NOVAK,¹ JEREMIAH P. OSTRIKER,¹ AND LUCA CIOTTI²

Draft version November 5, 2018

ABSTRACT

We extend the black hole (BH) feedback models of Ciotti, Ostriker, and Proga to two dimensions. In this paper, we focus on identifying the differences between the one-dimensional and two-dimensional hydrodynamical simulations. We examine a normal, isolated L_* galaxy subject to the cooling flow instability of gas in the inner regions. Allowance is made for subsequent star formation, Type Ia and Type II supernovae, radiation pressure, and inflow to the central BH from mildly rotating galactic gas which is being replenished as a normal consequence of stellar evolution. The central BH accretes some of the infalling gas and expels a conical wind with mass, momentum, and energy flux derived from both observational and theoretical studies. The galaxy is assumed to have low specific angular momentum in analogy with the existing one-dimensional case in order to isolate the effect of dimensionality. The code then tracks the interaction of the outflowing radiation and winds with the galactic gas and their effects on regulating the accretion. After matching physical modeling to the extent possible between the one-dimensional and two-dimensional treatments, we find essentially similar results in terms of BH growth and duty cycle (fraction of the time above a given fraction of the Eddington luminosity). In the two-dimensional calculations, the cool shells forming at 0.1–1 kpc from the center are Rayleigh–Taylor unstable to fragmentation, leading to a somewhat higher accretion rate, less effective feedback, and a more irregular pattern of bursting compared to the one-dimensional case.

1. INTRODUCTION

Nearly all massive galaxies are thought to harbor supermassive black holes (SMBHs), and the properties of the black holes (BHs) are known to be well correlated with those of their host galaxies (Gebhardt et al. 2000; Ferrarese & Merritt 2000; Tremaine et al. 2002; Novak et al. 2006; Gültekin et al. 2009). The direction of the causal link between SMBHs and host galaxy properties remains unclear, but the existence of such a correlation suggests an intimate connection between the physics of BH growth and galaxy formation. There has been intense theoretical interest in the ability of active galactic nuclei (AGNs) to affect the star formation histories and observed colors of galaxies (e.g., Di Matteo et al. 2005; Croton et al. 2006). There is certainly sufficient energy and momentum available to have a profound effect on the structure and dynamics of the interstellar medium (ISM).

Many physical processes can act to couple accretion by the central BH to the galaxy’s ISM. The most obvious and well-observed result of SMBH accretion is the prodigious luminous output. Radiatively efficient accretion converts a significant fraction of the rest mass energy of the infalling gas to radiation, and the bulk of the matter that enters BHs over the history of the universe is known to do so in a radiatively efficient manner (Soltan 1982). The emitted photons impart energy and momentum to the galaxy’s ISM via electron scattering, photoionization, scattering due to atomic resonance lines, and absorption by dust grains.

Accreting SMBHs are also known to drive broad ab-

sorption line (BAL) winds that convey mass, momentum, and energy to the surrounding galaxy. These winds are launched by electromagnetic processes within a few hundred gravitational radii of the central BH (e.g., Proga et al. 2000), but by the time the wind galactic length scales, the energy is carried by the kinetic motion of the gas. Only fraction of the energy output of the AGN will be converted to a wind, that wind will proceed to inject nearly all of its energy and momentum into the galaxy’s ISM. This high interaction efficiency has inspired strong theoretical interest in the effect of mechanical AGN feedback on galaxy properties (Di Matteo et al. 2005; Springel et al. 2005; Johansson et al. 2009).

The combined effect of these feedback processes can dramatically affect the galaxy and act to reduce subsequent SMBH accretion. Physical modeling of the complex processes involved is beginning to reach a level where observational tests of the models are possible. Building on previous work in one dimension (Ciotti & Ostriker 1997, 2001, 2007; Ciotti et al. 2009b; Shin et al. 2010; Ciotti et al. 2010), we perform two-dimensional simulations of SMBH accretion in the context of normal but isolated elliptical galaxies. Thus, the source of accreted gas is the fraction ($\sim M_*/6$) ejected into the ISM due to normal processed of stellar evolution, rather than the comparable amounts of gas added via cosmological infall. We take care to resolve the inner length scales of accretion (the Bondi radius) while also running the simulations long enough to resolve galactic length and timescales. Many physical processes must be included and numerically a large dynamic range is needed. Although quite well developed from the point of view of the included physics, our previous one-dimensional simulations obviously could not address the impact of genuinely two-dimensional phenomena on the feedback phenomenon. We recall here the most important of them,

¹ Department of Astrophysical Sciences, Peyton Hall, Princeton University, Princeton, NJ 08544, USA

² Department of Astronomy, University of Bologna, via Ranzani 1, I-40127, Bologna, Italy

that will be discussed in this paper.

The first one concerns the possible instabilities (e.g., Rayleigh–Taylor, RT) that can affect the evolution of the cold shells that appear during the evolution of one-dimensional models. The central bursts are caused by these shells, and the shells have a two-fold origin. At the beginning of each major burst, the classical Field cooling instability (Field 1965) appears around 1 kpc from the center, due to the local critical balance between heating and cooling. As the density increases, the shell starts to fall toward the center and compresses the gas. When a burst first appears, shock waves are sent from the center toward the falling shell, and a series of sub-bursts and consequent reflected shock waves impact on the cold shell, increasing its density still further. As the bulk of star formation in the one-dimensional models happens in these cold shells, it is very important to understand the cold shell physics, not only from the point of view of central accretion, but also for the starburst which occurs within the cold shell. From the short description above, a few obvious questions arise: for example, will the allowance of the additional degree of freedom still lead to a formation of a cold shell near the center in the case of an aspherical galaxy? What is the effect of non-zero angular momentum in the gas? Will the cold shell fall toward the center as in the one-dimensional simulations or it will break up due to (RT) instability? Even more important, what is the fate of the multiple interacting shocks? Will the accretion still be characterized by strong bursts separated by long time intervals or will the breakup of the shells lead to cold fingers of dense gas being accreted in a more or less steady flow while hot gas flows outward, therefore resulting in flows that at each radius are partially accreting and partially outflowing?

The second reason to move to two-dimensional simulations is to explore the interaction (and the consequent mechanical feedback) of the conical nuclear wind with the galaxy ISM. In our previous one-dimensional simulations this interaction was necessarily described as a spherical average of an inherently non-spherical effect, even though we had taken into account several physical aspects of the phenomenon via a time-dependent differential equation. Clearly, a two-dimensional simulation is also needed to explore Kelvin–Helmholtz instabilities at the interface between the outflowing conical wind and the ISM.

In the present work, we focus on two-dimensional simulations of a galaxy with very low specific angular momentum in order to make close contact with the existing one-dimensional simulations. We would like to isolate the effect of increasing the dimensionality of the simulation. The adopted angular momentum profile is consistent with the slowest of the SAURON slow-rotators (Emsellem et al. 2004). In future work, we will expand our treatment to include angular momentum transport via the standard α prescription (Shakura & Sunyaev 1973) and more recent models based on gravitational torques (Hopkins & Quataert 2010a).

There have been many numerical simulations of SMBH accretion and the subsequent effects on the galaxies containing the resulting AGN. Nearly all of the efforts to date can be classified into three broad categories. Di Matteo et al. (2005), Debuhr et al. (2010, 2011), and Johansson et al. (2009) are examples where the simu-

lations cover length scales from $\simeq 100$ pc to tens of kpc and timescales from a fraction of a Myr to several Gyr. Galactic length and timescales are resolved, but the SMBH accretion and feedback processes are considered to be sub-resolution. Complementary studies by Kurosawa & Proga (2009a) and Kurosawa & Proga (2009b) are examples of multi-dimensional simulations that cover the length scales from a few AU to $\simeq 1$ pc. Length and timescales relevant to SMBH accretion are resolved, and the generation of radiatively driven winds is computed, but these simulations do not approach galactic length or timescales, and infall rates are taken as given. Hopkins & Quataert (2010b) and Levine et al. (2008) are examples of a multi-resolution studies of SMBH accretion involving progressively higher spatial resolution simulations run for progressively shorter times. The highest spatial resolution simulations go down to a fraction of a pc and are run for about one Myr of simulation time. These simulations spatially resolve the accretion process, but do not reach galactic timescales. Therefore, they cannot self-consistently calculate the effect of AGN feedback on the gas in the galaxy as a whole and the subsequent SMBH accretion.

Finally, there have been several numerical studies of accretion by intermediate-mass black holes (IMBHs) with the goal of understanding BH growth in the early universe (Alvarez et al. 2009; Park & Ricotti 2010). In terms of dimensionless length scales r/r_{Bondi} or $r/r_{\text{Schwarzschild}}$, some of these simulations are similar to our simulations. However, studies of IMBH accretion focus on BHs with very small masses ($100\text{--}1000 M_{\odot}$) compared to those presented here. Therefore, the relevant physical length and timescales are much smaller and the physical sources of the infalling gas are very different from those considered in the present work.

Our goal is to resolve both the relevant accretion length and timescales while at the same time resolving galactic length and timescales (cf. Levine et al. 2008; Alvarez et al. 2009). There have been only a few attempts to perform multi-dimensional simulations that bridge the gap between galactic and SMBH scales, although several papers have examined the interaction between an outflowing wind/jet with specified properties and the surrounding intergalactic medium (cf. Metzler & Evrard 1994; Omma & Binney 2004; Sijacki et al. 2007; Sternberg & Soker 2008; Reeves et al. 2009; Fabian et al. 2009; Arieli et al. 2010)

The present work is an attempt to simultaneously resolve the inner length scales relevant to SMBH accretion (a few pc), outer length scales relevant to galaxies (tens of kpc), inner timescales relevant to SMBH accretion (a few years), and outer timescales relevant to galaxies and stellar evolution (10 Gyr). However, the region inside of 1 pc including the disk and the SMBH itself are still treated as sub-resolution physics and we compute the output from these regions as time-dependent functions of the input to them, utilizing formulae from the above quoted sources.

We take particular care to resolve the inner scales where the rate of accretion is set (the Bondi radius) even for the hot gas in the system. This is important because heating due to AGN radiation or mechanical energy input may raise the gas temperature as it falls toward the SMBH, decreasing the relevant Bondi radius. For exam-

ple, Alvarez et al. (2009) performed cosmological simulations of accretion onto the SMBH left by the first stars at high redshift. Their resolution was sufficient to resolve the Bondi radius for the cold gas in their simulation, but not for the much hotter gas affected by feedback. This means that if the heating would have been effective between the resolution of their simulation and the actual hot-gas Bondi radius, then in reality the gas would never have made it to the SMBH. It is important to realize that the material emitted by the evolving stars (the fuel for SMBH accretion) is thermalized by stellar velocity dispersion to the equivalent temperature, and that the stellar velocity dispersion near the BH increases (as $1/r$ in the isotropic case). Therefore, the gas is injected at higher and higher temperature approaching the central BH and the location of the Bondi radius does not change significantly even if the SMBH grows in mass. Care must be exercised in the numerical treatment of the central regions. To put it simply, Bondi-type accretion cannot be computed properly unless the detailed thermal state of the gas is followed to well within the radius at which gravitational and thermal energies are balanced.

Section 2 describes the simulations and our basic approach, Section 3 gives our results, and Section 4 summarizes our conclusions.

2. METHODS

We use the Zeus hydrodynamics code (Stone & Norman 1992) because of its ability to utilize spherical geometry and variable cell sizes. The code is not adaptive in the sense that it does not dynamically decide where to place extra cells, but the variable cell sizes allow us to identify a center of interest and take advantage of increased resolution near that point. We extend the code with mass, energy, and momentum source terms appropriate for stellar evolution in elliptical galaxies, SMBH accretion, and feedback resulting from the accretion, following the treatment described in Ciotti et al. (2009b).

The simulation grid is the meridional plane in spherical coordinates where all quantities are assumed to be axisymmetric. The radial bins are the same as in the one-dimensional simulations: 120 cells covering 2.5 pc to 250 kpc where each cell is 10% larger than the previous cell. Requiring the cells to have an aspect ratio of unity gives 30 angular cells. We exclude the region from 0 to 0.05 radians near either pole because cell volumes go to zero due to the coordinate singularity there.

The simulations are not limited by the total volume of computation required, but rather by the time to solution. The Courant–Friedrich–Levy (CFL) condition for the central grid cells is quite severe: time steps are $\simeq 10$ years, and we would like to run the simulation for 12 Gyr. Numerical schemes which allow the time step to increase with increasing radius could be implemented, but the estimated speedup is quite limited. For a single processor this would save a factor of $N_r(1-(r_i/r_o)^{1/N_r}) \simeq 10$ where N_r is the number of grid cells in the r -direction, r_i is the innermost radius, r_o is the outermost radius, we have assumed log-spaced bins in radius, and the numerical value is for our chosen parameters of $r_i/r_o = 10^{-5}$ and $N_r = 120$. In a multi-processor environment, the reduction in wallclock-time is given by the same formula with r_i, r_o , and N_r referring to the cells on a given processor

rather than the whole simulation. For our simulations running on eight processors, the speedup would be only $\simeq 40\%$.

As the mass of the central SMBH increases, one might think that the Bondi radius increases so that a moving inner grid could help in speeding up the simulations. As discussed above, this will not work since the gas losses from the evolving stars near the SMBH are thermalized at the local value of the velocity dispersion, which increases with BH mass. In practice, the location of the “Bondi radius” remains approximately fixed for the entire time of the simulation, and varies chiefly due to fluctuations in the local speed of sound caused by feedback from the SMBH and by the accretion of cold gas.

Our requirements for the spatial resolution near the center of the simulation, the amount of time for which the simulation must run, and the CFL condition near the center have constrained us to use a rather small number of cells. We have performed a few simulations where the number of grid cells is doubled in each dimension, and the simulation ran for ~ 1.3 Gyr rather than 12 Gyr. Most physical quantities did not change significantly. The exception was the change in the BH mass, which was a factor of two larger. Smaller cells allow denser blobs and filaments to form, which have an easier time making their way to the center of the simulation. It is also important to note that the size of the cells grows linearly with radius so that physical structures of constant size (e.g., molecular clouds) will be resolved progressively more poorly further from the center of the simulation.

2.1. Physics

For the most part the input physics is the same as that described in Ciotti et al. (2010) with a few exceptions described in detail below. A complete description of the input physics is given in Ciotti & Ostriker (2007), Ciotti et al. (2009b), and Sazonov et al. (2005). Here we repeat the most important aspects.

The total gravitational potential of the model galaxy is assumed to be a singular isothermal sphere plus a point mass for the central BH. This is good agreement with recent observations of the total mass profile of early-type galaxies (Gavazzi et al. 2007, 2008). For simplicity we maintain this model in to the smallest radii, although more complicated models may be more appropriate inside of a fraction of the half-light radius. The velocity dispersion parameter of the isothermal potential is 260 km s^{-1} . The gas is not self-gravitating.

The stellar distribution is given by a Jaffe profile with a total mass of $3 \times 10^{11} M_\odot$ and a projected half-mass radius of 6.9 kpc. The mass-to-light ratio is assumed to be spatially constant and is equal to 5.8 in solar units in the B band at the present time.

Energy and mass input due to stellar evolution, type Ia supernovae, star formation, type II supernovae are exactly the same. The specific energy of the material provided by stellar evolution is calculated according to the solution of the Jeans equation for the given stellar density distribution and gravitational potential as given in Ciotti et al. (2009a). Gas heating and cooling due to atomic processes as well as Compton heating and bound-free absorption of radiation from the AGN are calculated using the formulae from Sazonov et al. (2005), as in Ciotti et al. (2010).

Gas temperatures are bounded from below by the fact that our atomic cooling curve has an exponential cutoff below 10^4 K and from above by our assumed broad-line wind velocity of $10,000 \text{ km s}^{-1}$, corresponding to 2.5×10^9 K if all of the kinetic energy is converted to thermal energy. However, this very hot gas will always be strongly outflowing until it distributes its energy to a much larger mass of gas so that the temperature is of order the virial temperature of the halo. The upper temperature bound for infalling gas is given by the maximum temperature to which the AGN photons can heat the gas. This is given by the Compton temperature, which we take to be $2.1 \text{ keV} = 2.5 \times 10^7 \text{ K}$ (Sazonov et al. 2005).

Star formation is implemented using the standard Schmidt–Kennicutt prescription. The star formation rate density is given by

$$\dot{\rho}_* = \frac{\eta_{\text{form}} \rho}{\tau_{\text{form}}}, \quad (1)$$

where ρ is the local gas density, $\eta_{\text{form}} = 0.1$ is a dimensionless parameter for the rapidity of star formation and

$$\tau_{\text{form}} = \max(\tau_{\text{cool}}, \tau_{\text{dyn}}) \quad (2)$$

$$\tau_{\text{cool}} = E/C \quad (3)$$

$$\tau_{\text{dyn}} = \min(\tau_{\text{jeans}}, \tau_{\text{rot}}) \quad (4)$$

$$\tau_{\text{jeans}} = \sqrt{\frac{3\pi}{32G\rho}} \quad (5)$$

$$\tau_{\text{rot}} = \frac{2\pi r}{v_c(r)}, \quad (6)$$

where E is the internal energy per unit volume of the gas, C is the volumetric cooling rate, G is the Newtonian gravitational constant, r is the distance from the center of the galaxy, and $v_c(r)$ is the circular velocity as a function of radius. Type II supernovae then return mass and energy to the ISM such that the mass returned is 20% of that processed through stars and the energy is $E_{\text{SN}} = 4 \times 10^{-6} \dot{m}_{\text{SF}} c^2$. These values for the energy and mass returned result from our assumption of a Salpeter initial mass function with a low-mass cutoff of $0.1 M_{\odot}$, together with our assumption that every star above $8M_{\odot}$ injects its entire mass and 10^{51} erg into the ISM.

In the momentum equation, the force exerted on gas due to Compton scattering of photons from the AGN is treated as in the one-dimensional code. Note that because the vast majority of the photons from the AGN have energies far below the electron rest mass energy, Compton scattering takes place in the coherent limit where photon energies and numbers are preserved. Therefore, in both the optically thin and optically thick limits, the force per unit mass on a fluid element is

$$F/m = \frac{\kappa_{\text{ES}} L(r)}{4\pi r^2 c}, \quad (7)$$

where κ_{ES} is the electron scattering opacity and $L(r)$ is the total luminosity emitted interior to r (that is, there is no $e^{-\tau}$ factor, where τ is the optical depth).

The force exerted by absorption of AGN photons by atomic lines is also the same as in the one-dimensional code: $dp/dt = l/c$, where l is the energy absorbed per unit time in a given cell. In the work reported on in

this paper, the radiation momentum associated with dust absorption (cf. Debuhr et al. 2011) is not included in the two-dimensional calculation although it is included in the one-dimensional treatment.

Some physical processes are modeled using the same basic assumptions as in the one-dimensional code, but two-dimensional simulations allow us to improve the implementation.

This is the case with the BAL wind. The one-dimensional and two-dimensional simulations use the same formulae to compute the total mass, momentum, and energy injected into the ISM for a given SMBH accretion rate. However, the one-dimensional simulations use a prescription based on pressure balance between the outgoing wind and the ambient gas in the galaxy in order to compute how the mass, energy, and momentum are radially distributed. In the two-dimensional simulations, we can adopt the more realistic treatment of simply injecting the desired mass, energy, and momentum into the innermost radial cells and self-consistently computing the radial transport of these quantities.

The one-dimensional code specifies the opening angle of the wind for the purpose of solving for the radial distribution of the deposited material. The two-dimensional code requires a more precise specification of the dependence of the outflowing material on angle from the pole. We choose the simple parameterization:

$$\frac{dq}{d\theta} = \frac{(n+1) \sin \theta |\cos^n \theta| Q}{4\pi}, \quad (8)$$

where q is a conserved quantity (mass, energy, or radial momentum), Q is the total amount of the conserved quantity to be injected. We solve for n such that the angle θ enclosing half of the conserved quantity is the same as the opening angle specified in the one-dimensional code. For the fixed-opening-angle models considered here, $n = 2$, so that the half-opening angle enclosing half of the energy is $\sim 45^\circ$. In terms of solid angle, this means that the wind is visible from $\sim 1/4$ of the available viewing angles. This fraction is in agreement with observations of the fraction of obscured and unobscured AGNs under the assumption that the two populations are made up of a single population of objects that differ only in viewing angle.

Finally, some processes of minor importance have been omitted from the two-dimensional simulations so far. This includes the prescription for star formation and stellar remnant formation in the central sub-grid SMBH accretion disk. The two-dimensional code implements no star formation in the disk—all gas that flows in eventually either flows into the SMBH or back onto the simulation grid as a conical wind.

The major difference between the calculations presented here and the one-dimensional models is that the two-dimensional models do not yet implement any optically thick radiative transfer algorithms. We assume that the gas is always optically thin at all wavelengths at all times. There is also no treatment of the temperature dependence of dust opacity. Finally, the radiation pressure due to stars formed in the simulation is also omitted from the momentum equation.

Experiments using one-dimensional models have shown that omitting the radiation pressure on dust does not

greatly affect the overall SMBH mass growth when these other feedback mechanisms are included (less than a factor of two). However, star formation can be affected because infalling cold shells can have their falling time extended by radiation pressure on dust, allowing more stars to form as the gas is falling. Improving the treatment of radiative transfer in the two-dimensional code will be the subject of future work.

Computational efficiency requires that we limit the velocities and sound speeds in the simulation to prevent the CFL condition from restricting the time step too dramatically. At the high end, we impose a limit of 30,000 km s⁻¹ on the gas velocities and sound speeds. The source term with the highest specific energy is the mechanical wind due to SMBH accretion, which injects gas at 10,000 km s⁻¹. The limit is three times higher, corresponding to 10 times the energy density, so this limit should not greatly affect overall evolution of the system.

In the one-dimensional simulations, we imposed the commonly used requirement that the ISM temperature be above 10⁴ K. This was necessary because the one-dimensional code uses a fully explicit time integration scheme and low thermal energies imply exceedingly short cooling times. In the two-dimensional calculations, we use a semi-implicit time integration method, making it possible to set the lower bound on temperature at a lower value. We impose three limits dictating that the gas does not drop below the temperature of the cosmic microwave background, the effective temperature associated with the AGN radiation field or the effective temperature of the stellar radiation field. The two-dimensional simulations make use of the same cooling curve as the one-dimensional simulations, which has an exponential cutoff below 10⁴ K. Therefore, gas cannot reach these low temperatures by cooling alone, but must undergo a dramatic expansion. This occasionally occurs due to the violent gas motions near the center of the simulation.

We calculate the temperature of the cosmic microwave background assuming an Einstein–de Sitter universe with an age of 13.7 Gyr where the beginning of the simulation corresponds to 1.7 Gyr after the big bang. The difference between an Einstein–de Sitter universe and the standard Λ CDM cosmology is minimal for our present purpose.

The effective temperature of the photons from the AGN is just

$$T = \left(\frac{L}{4\pi c a r^2} \right)^{1/4}, \quad (9)$$

where $a = 8\pi^5 k_B^4 / 15c^3 h^3$ is the radiation constant.

It is easy to show that for a spherically symmetric distributed luminosity source, the energy density in the photon field at R is

$$e(R) = \int_0^\infty \frac{j(r) dr}{2cR} \log \frac{R+r}{|R-r|}, \quad (10)$$

where $j(r)$ is the luminosity per unit volume.

However, we adopt the expression

$$e(R) = \int_0^\infty \frac{r^2 j(r) dr}{c(r^2 + R^2)} \quad (11)$$

because it gives simple analytic integrals and has the correct form in the limits when $r \gg R$ and $r \ll R$. The integrand of Equation (11) underestimates the integrand of

Equation (10) when r is near R . However, the difference between the two expressions is less than 30% provided that r and R differ by at least a factor of two. Given that $l(r)$ is typically a steeply falling function of r , the integral is not typically dominated by the region where $r \sim R$.

For the present case of a Jaffe profile assuming a constant stellar mass-to-light ratio, this gives

$$e(R) = \frac{L}{4\pi c R^2} \frac{y(y^2 - 2y \log y - 1)}{(y-1)^3}, \quad (12)$$

where $y = R/r_*$, r_* is the scale radius from the Jaffe profile, L is the total luminosity, and the expression has a finite limit when $y = 1$.

There are also some minor computational differences between the two codes. The one-dimensional simulations use a fully explicit algorithm for time integration. In the two-dimensional code, the time integration is mostly explicit, but we use a semi-implicit scheme for radiative cooling because the cooling timescales can become very short. If the time step required by the CFL condition is shorter than the cooling time, the code updates gas temperatures due to radiative cooling explicitly. If the cooling time is shorter than the CFL time step, the code evaluates the cooling function at the advanced time, using a bisection algorithm to find the root of the resulting equation for the gas temperature at the advanced time.

2.2. AGN Feedback Parameterization

The BAL originating near the SMBH provides energy, momentum, and mass from a wind to the ISM according to the equations:

$$\dot{M}_{\text{BH}} = \dot{M}_{\text{infall}} / (1 + \eta), \quad (13)$$

$$\eta = 2\epsilon_W c^2 / v_W^2, \quad (14)$$

$$\dot{E}_W = \epsilon_W \dot{M}_{\text{BH}} c^2, \quad (15)$$

$$\dot{P}_W = 2\epsilon_W c^2 \dot{M}_{\text{BH}} / v_W, \quad (16)$$

and

$$\dot{M}_W = 2\epsilon_W c^2 \dot{M}_{\text{BH}} / v_W^2, \quad (17)$$

where v_W is the velocity of the BAL, taken here to be 10,000 km s⁻¹. As discussed in detail in Ostriker et al. (2010), these expressions guarantee that the mass, energy, and momentum carried by the wind are self-consistent.

Ciotti et al. (2009b) considered two classes of mechanical feedback, denoted the A and B models. For the A models, both the mechanical efficiencies and the wind opening angles were independent of the accretion rate. The B models have mechanical efficiencies and wind opening angles that varied with SMBH accretion rate such that both quantities are small at small accretion rate and reach a specified maximum at the Eddington rate.

Independently of the mechanical feedback model, the radiative luminosity of the AGN is given by

$$L = \epsilon_{\text{EM}} \dot{M}_{\text{BH}} c^2, \quad (18)$$

where the electromagnetic efficiency is given by the advection dominated accretion flow inspired (Narayan & Yi

1994) formula:

$$\epsilon_{\text{EM}} = \frac{\epsilon_0 A \dot{m}}{1 + A \dot{m}}, \quad (19)$$

and $A = 100$ and $\epsilon_0 = 0.1$. The dimensionless mass accretion rate is

$$\dot{m} = \frac{\dot{M}_{\text{BH}}}{\dot{M}_{\text{Edd}}} = \frac{\epsilon_0 \dot{M}_{\text{BH}} c^2}{L_{\text{Edd}}}, \quad (20)$$

where L_{Edd} is the Eddington luminosity.

The mechanical wind efficiency is given by ϵ_W = constant for A models. The specific parameters for the simulations presented here are given in Table 1. The present work considers two-dimensional analogs of the simpler A models only.

We also ran two-dimensional analogues of the Ciotti et al. (2009b) B models where the mechanical feedback efficiency falls off at low Eddington ratios (as expected from computational studies of the creation of BLWs in the inner few hundred gravitational radii (Kurosawa & Proga 2009a; Kurosawa et al. 2009; Kurosawa & Proga 2009b)). In one dimension, mechanical feedback in the B models was sufficient to regulate the SMBH growth. However, in two dimensions equivalent models were found to undergo too much SMBH growth and had distributions of Eddington ratios very different from those observed for actual galaxies. Comparing one-dimensional and two-dimensional A models reveals that feedback is less effective in two dimensions: more energy is required for the SMBH to effectively regulate its growth. For two dimensions, the low efficiencies at low Eddington ratio combined with the diminished effectiveness of feedback in two dimensions make the two-dimensional B models observationally unacceptable.

The model most similar to that used by Di Matteo et al. (2005) is A0. The model has an efficiency of 5×10^{-3} , but we take into account the fact that the wind carries not only energy but also momentum and mass into the ISM. Matching our momentum input rate to that used by Debuhr et al. (2011) gives $\epsilon_W = v_w \epsilon_0 \tau / 2c \simeq 0.04$, where $\tau = 25$ is their chosen wavelength-averaged optical depth parameter and $v_w = 10,000 \text{ km s}^{-1}$ is our chosen BAL wind velocity parameter. The present models do not include a simulation with such a high feedback efficiency. Our model that most closely approximates those of Debuhr et al. (2011) is again A0, with the caveat that we inject less momentum for the same BH luminosity. Note that Debuhr et al. (2011) effectively assume a much lower wind velocity (not intended to model BAL winds) and as a result the energy actually injected into the ISM in their simulations is similar to that used in Di Matteo et al. (2005). The above considerations are intended to determine what parameters we would need to adopt for our present simulations in order to produce models similar to existing ones by other authors given our assumed BAL velocity. A closer study of the similarities and differences between these AGN feedback models is the subject of a forthcoming paper.

2.3. Angular Momentum

The one-dimensional simulations did not permit the simulated gas to have non-zero angular momentum. The

two-dimensional simulations assume axisymmetry and compute the velocity in the ϕ -direction. We must assume an angular momentum profile for the injected gas. In the present simulations, we avoid forming a rotationally supported gas disk by choosing the radius of centrifugal support to be inside the innermost grid cell.

This assumption gives rotation velocities comparable to the slowest of the SAURON slow-rotators (Emsellem et al. 2004, 2007). Thus, our model galaxy is representative of a rather small set of observed galaxies. However, the advantage of assuming very little rotation is that it allows us to avoid specifying an ad hoc prescription for angular momentum transport. The low angular momentum case also allows the closest comparison to the existing one-dimensional simulations, allowing us to isolate the effect of dimensionality. In future work we plan to implement standard recipes for angular momentum transport, including an α disk (Shakura & Sunyaev 1973) and models based on gravitational torques (Hopkins & Quataert 2010a). Taking angular momentum transport into account is likely to have a significant effect on our computed results. Our consideration of the low angular momentum case will facilitate isolating the effect of angular momentum in future analysis.

The assumed net specific angular momentum of the stars providing gas in the simulation is thus taken to be given by

$$\frac{1}{v_\phi(R)} = \frac{d}{\sigma R} + \frac{1}{f\sigma} + \frac{R}{j}, \quad (21)$$

where v_ϕ is the velocity in the azimuthal direction, R is the distance to the z -axis, σ is the central one-dimensional line-of-sight velocity dispersion for the galaxy model, and d , f , and j are adjustable parameters controlling the angular momentum profile at small, intermediate, and large radii, respectively. This parameterization gives solid body rotation at radii less than d and constant specific angular momentum of j at large radii. The second term on the right prevents the rotational velocity from exceeding $f\sigma$ at any radius. If there is a range of values of R for which the $f\sigma$ term dominates, then is a region of intermediate radii with constant rotational velocity.

2.4. Initial Conditions

The initial conditions are chosen to match those of the one-dimensional simulations, fully described in Ciotti et al. (2010). Briefly, the total gravitational potential is that of a singular isothermal sphere with one-dimensional velocity dispersion 260 km s^{-1} and with a central point mass with initial mass $3 \times 10^8 M_\odot$. The stellar distribution is a Jaffe profile with projected half-light radius 6.9 kpc , mass-to-light ratio 5.8 in solar units, and total mass $3 \times 10^{11} M_\odot$. These parameters are chosen to put the initial galaxy on the Fundamental Plane (Djorgovski & Davis 1987; Dressler et al. 1987), the Faber–Jackson (1976) relation, and the Magorrian et al. (1998) relation. All of the relevant dynamical properties of the galaxy models are given in Ciotti et al. (2009a). The gas density is initially set to a very low value so that the gas in the simulation comes almost exclusively from explicit source terms arising from stellar evolution.

2.5. Boundary Conditions

We assume reflecting boundary conditions on the θ boundaries occurring at either pole. On the outer radial boundary we assume that all fluid quantities are constant. This allows both outflow and inflow depending on the state of gas just inside the outer boundary.

On the inner radial boundary we assume reflecting boundary conditions if the innermost radial velocity is positive. Physical processes that inject mass (such as the BAL wind) are handled as explicit source terms acting in the first set of radial cells. This allows us to easily handle the cases of very strong, very weak, and intermediate flows of energy, mass, and momentum onto the computational grid with a single source term. If the innermost radial velocity is negative, we use an outflow (off of the computational grid toward the center of the simulation) boundary condition where all fluid variables are constant across the boundary. The one exception in this case is the radial velocity itself. If the cell is inside the locally estimated Bondi radius (that is, the Bondi radius has been resolved), then no limit is imposed upon the inflow velocity. However, if the cell is outside the locally estimated Bondi radius (the Bondi radius is unresolved), then the radial velocity is limited to the velocity that would result in mass transport consistent with the Bondi accretion rate. That is

$$v_{r,0} = \begin{cases} 0 & : \text{if } v_{r,1} > 0 \\ v_{r,1} & : \text{if } v_{r,1} < 0, r_1 < r_B \\ (r_B/r_1)^2 v_{r,1} & : \text{if } v_{r,1} < 0, r_1 > r_B. \end{cases} \quad (22)$$

As discussed above, we are careful to resolve the Bondi radius even for gas heated to the maximum expected temperature for infalling gas, the Compton temperature. However, the BAL wind has an even higher specific energy. Typically, the BAL wind is flowing strongly outward and the Bondi radius is always resolved. However, it is possible for the wind to fill the inner region of the galaxy with gas heated above the Compton temperature. In this case, Equation (22) ensures that the SMBH accretion rate is reduced accordingly.

It is unfortunately not possible to cleanly separate the SMBH scales from the galactic ones. Physically, this is because the source of gas in the galaxy is the stars, evolving on galactic timescales. Meanwhile, the SMBH is easily able to affect gas on kiloparsec scales. This ties the scales together in a feedback loop that cannot be easily separated into two separate simulations, or a simulation plus a sub-grid model. Furthermore, the classic Bondi solution is for the simple case of a point mass. If the mass enclosed by the Bondi radius is dominated by the galaxy rather than the central BH, then the classic Bondi solution is modified, particularly if the galactic mass is not spherically symmetric.

3. RESULTS

The character of the SMBH accretion changes dramatically in going from one to two dimensions. In one dimension, accretion events happen when a cold shell of gas forms at $\simeq 100$ pc. The shell falls into the SMBH as a unit and, after a series of sub-bursts in which direct and reflected shock waves interact and carry new material for accretion on the SMBH, triggers a dramatic release of energy from the SMBH. This leaves a sphere

of hot gas at the center of the simulated galaxy. Subsequent cold shells can only reach the center when the gas beneath them either cools or is compressed inside the innermost grid point. The hot gas generated by radiative and mechanical AGN feedback is able to prevent SMBH accretion until it cools. These processes lead to dramatic bursts followed by long, extremely quiet periods, spaced by the cooling time of the central gas. As the collapsing cold shell sits on top of hot and low density gas, it was already clear from the previous one-dimensional simulations that the shells are RT unstable.

In two dimensions, cold gas forms again at $\simeq 100$ pc. However, cold gas takes the form of rings rather than shells due to the classical RT instability. Shells sometimes form, but they fragment quickly. If there is hot gas beneath the cold ring, both the RT and convective instabilities operate to allow the cold gas to fall to the center of the simulation unimpeded. These instabilities cannot operate in one dimension. In two dimensions, they allow both higher and more chaotic SMBH accretion rates.

Figure 1 shows the simulation during a relatively quiet period. Figure 2 shows the start of an accretion event. A cold blob of gas is freely falling to the center of a two-dimensional simulation. Figure 3 shows a simulation snapshot just after an accretion event with the bipolar BAL wind flowing away from the center of the simulation. Gas is able to continue to fall into the SMBH via the simulation midplane. Finally, Figure 4 shows a simulation snapshot significantly after an accretion event (but not so long that the galaxy is able to return to a quiescent state). Dense overlying gas has caused the BAL wind to become nearly isotropic, making additional accretion via the midplane impossible.

3.1. Black Hole Growth

Figure 5 shows SMBH mass versus mechanical feedback efficiency for one- and two-dimensional A models as well as one-dimensional B models. The SMBHs undergo more growth in two dimensions at a fixed feedback efficiency owing to RT instabilities, making it easier for cold gas to fall in.

3.2. Time Dependence of SMBH Accretion

The character of the time dependence of SMBH accretion is much different in two dimensions than in the one-dimensional case. In one dimension, SMBH accretion occurs in a few bursts well separated in time. Occasionally a given burst will have a complex character, being composed of many sub-bursts. In two dimensions, there are still occasionally events that can be characterized as bursts followed by quiescent periods. However, the quiescent periods are shorter and the SMBH is more active during them compared to the one-dimensional case. Furthermore, during times far from a major burst when gas is building up in the galaxy, the SMBH is far more active than in the one-dimensional case and the accretion takes on a stochastic character.

Figure 6 shows the Eddington ratio L/L_{Edd} as a function of time for part of the A2 simulation. The SMBH accretion is much more chaotic than in the one-dimensional case. In the one-dimensional case, a cold shell forms and falls in as a unit only after the gas interior to it has also cooled. In two dimensions, these same cold shells form,

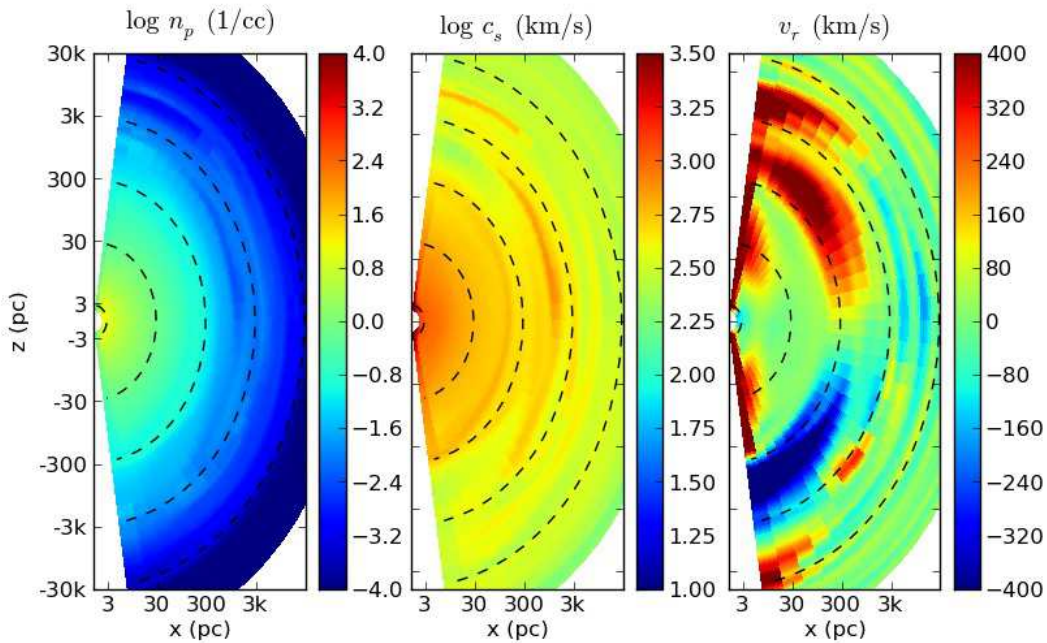


FIG. 1.— Simulation snapshot during a quiescent period. On the left, gas density in number of protons per cubic centimeter. In the center, log sound speed in kilometers per second. On the right, the radial velocity in kilometers per second. The x - and y -axes are logarithmic in the distance to the SMBH. Outflowing gas from past accretion events is visible from 300 pc to 10 kpc. Persistent low-level accretion maintains a narrow continuous outflow near the poles.

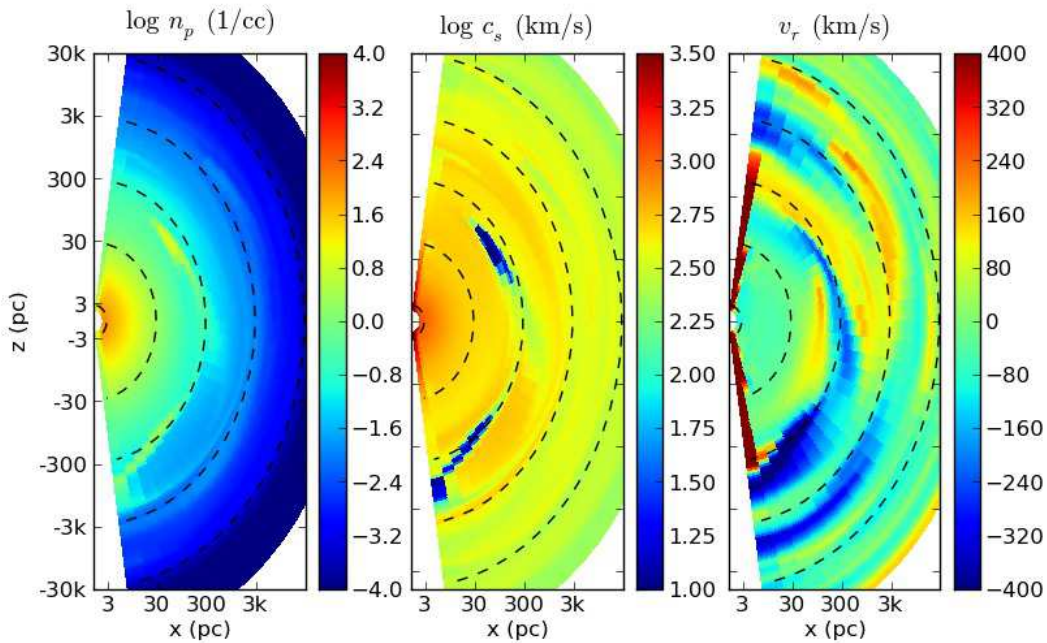


FIG. 2.— Snapshot from an axisymmetric simulation showing a cold blob falling to the center of the galaxy. The cold gas was produced by enhanced cooling in an overdense quasi-spherical shell with a covering fraction of about one-third of the sphere. The gas quickly collapses to a ring with a small covering fraction and/or fragments as it freely falls to the center of the simulation.

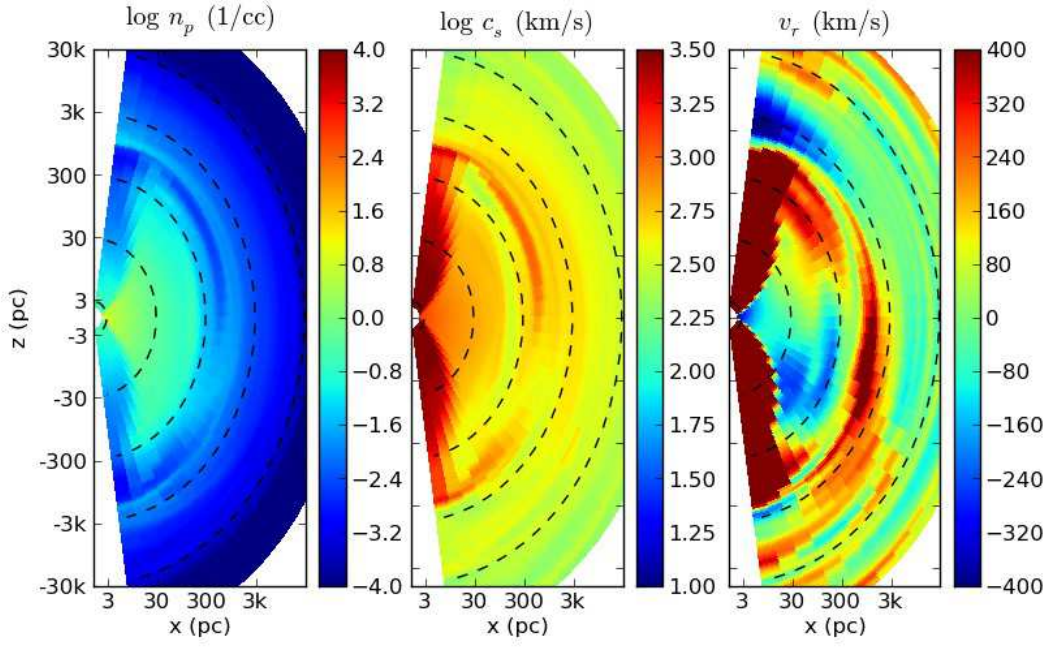


FIG. 3.— Simulation snapshot during an accretion event. A significant quantity of hot, outflowing gas injects energy and momentum into the interstellar medium at $r \simeq 1$ kpc.

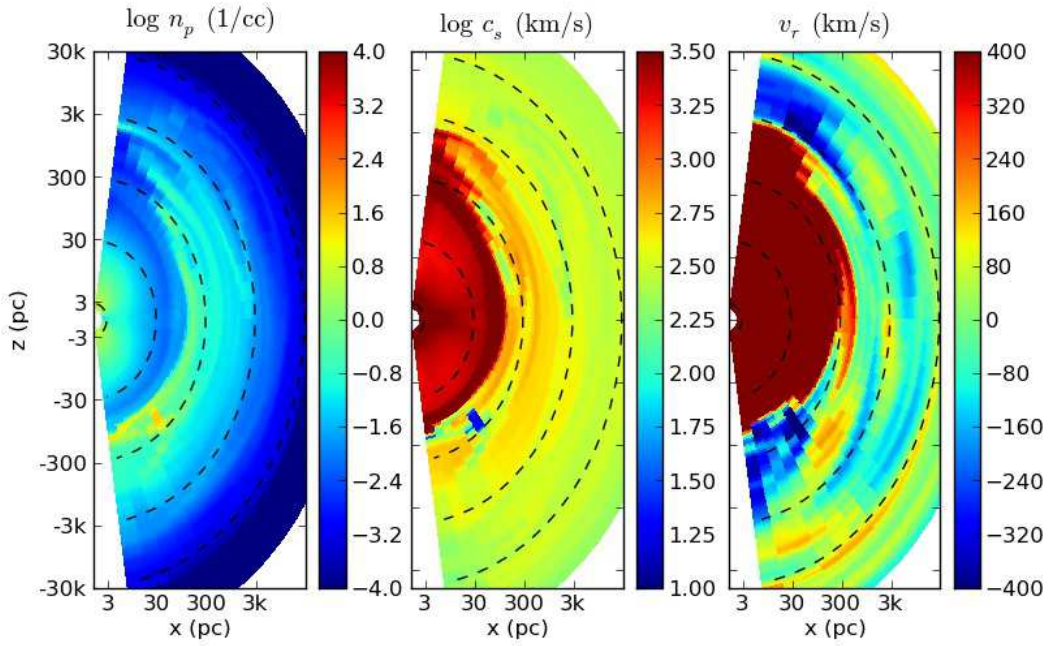


FIG. 4.— Simulation snapshot showing the final stages of a major accretion event. A hot, expanding bubble of gas extends to 100 pc, shutting down further SMBH accretion. Dense, overlying gas has caused the initially bipolar BAL wind to become quasi-spherical. The hot bubble is breaking through the overlying gas in at the north pole, which will lead to a unipolar wind.

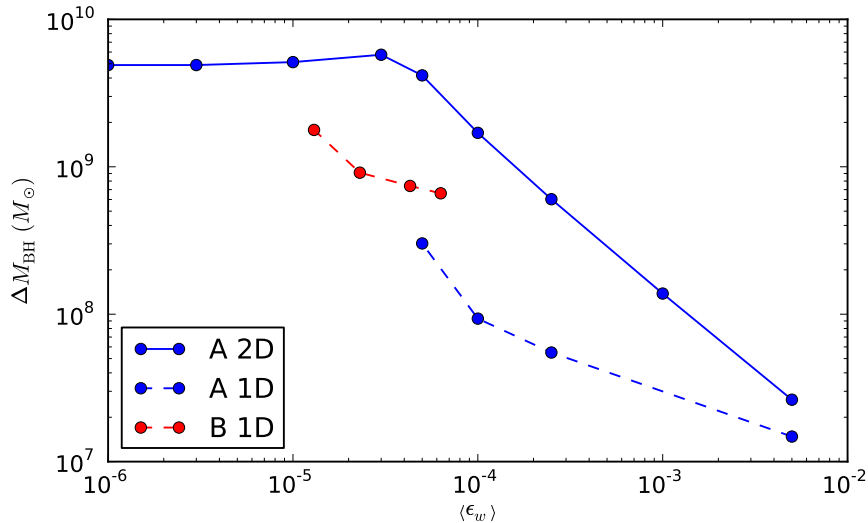


FIG. 5.— Final SMBH masses vs. mass-averaged wind Efficiency for one- and two-dimensional A models. The low-efficiency two-dimensional models produce SMBHs at the upper end of the range of observed central SMBHs for the characteristics of our model galaxy. Two-dimensional models allow more SMBH growth at a given efficiency because instabilities allow cold shells of gas to break up and fall into the center of the simulation with greater ease than in the one-dimensional case. A more accurate two-dimensional treatment of the radiative transfer in optically thick regions would probably lead to a reduction in the SMBH masses.

but they immediately break up into blobs that are RT unstable. The cold blobs fall in to the SMBH on a free-fall time in a much more disorganized fashion compared to one dimension.

Figure 7 shows the power spectrum of the Eddington ratio as a function of time for the A2 simulation. In spite of the complex, detailed implementation of the physics of stellar evolution, atomic cooling, star formation, supernovae, and AGN feedback, the power spectrum reveals a simple, gently sloped power law (roughly frequency to the one-fourth power) at low frequencies. At high frequencies, the power spectrum falls off as $1/f$ because of the filtering effect of the SMBH accretion disk.

Figure 8 shows the cumulative distribution of Eddington ratios for the A2 simulation. The black (red) lines show the cumulative time the simulation spends above (below) the given Eddington ratio. Solid lines show the cumulative distribution of Eddington ratios for the entire simulation, while the dashed lines show the distribution for the final 2 Gyr (corresponding to low redshifts). Low-redshift observational constraints for the fraction of $3 \times 10^8 M_\odot$ BHs accreting at 1% and 10% of the Eddington rate are taken from Heckman et al. (2004), Greene & Ho (2007), Ho (2009), and Kauffmann & Heckman (2009). A constraint on the fraction of high-redshift Lyman-break galaxies showing nuclear activity is taken from Steidel et al. (2003).

There is reasonable agreement between the simulations and observational constraints for a mechanical efficiencies ϵ_W between 10^{-3} and 10^{-4} . This range is in agreement with the recent study by Arav et al. (2011). They presented new observations as well as values drawn from the literature for \dot{E} and \dot{M} for five broad-line systems. The mean value of $\log \epsilon_W$ for the five systems is -4.2 with a mean error of 0.2 dex for each system and a standard deviation of 0.4 dex for the five points.

3.3. Disk Wind Opening Angle

The opening angle of the disk wind is expected to have an effect on the SMBH growth by controlling the effectiveness of the AGN feedback. At very small opening angles, the energy injected by the SMBH drills through the nearby gas and exits the central region as a narrow beam. All of the energy is eventually deposited at radii beyond one kpc, leaving the cooling and infalling gas in the central region essentially undisturbed. This should result in large SMBH growth.

As the opening angle increases, one might expect that mechanical feedback would become more and more effective as the wind interacts with an increasingly large fraction of the gas surrounding the SMBH. This would imply that isotropic feedback would result in the least SMBH growth.

Figure 9 shows final SMBH masses versus wind opening angle. The largest SMBH growth occurs when the wind is isotropic. A very wide opening angle allows the wind to effectively couple to all of the gas at small radius, temporarily suppressing SMBH accretion. However, the wind's outward progress is soon stopped because the wind must essentially lift the entire overlying gaseous atmosphere. The wind is not able to move a significant amount of gas to a sufficiently large radius to prevent eventual accretion onto the SMBH.

This implies that there is an opening angle that results in minimal SMBH growth. The angle will likely be a function of the mechanical feedback efficiency as well as the other physical parameters for the gravitational potential, stellar distribution, mass-loss rates, and so forth. Figure 9 shows the increase in SMBH growth at large opening angles, but does not show evidence for the expected increase in SMBH growth as the opening angle becomes very small. However, it is worth noting that the change in BH mass growth is less than a factor of two for a wide range of wind opening angles.

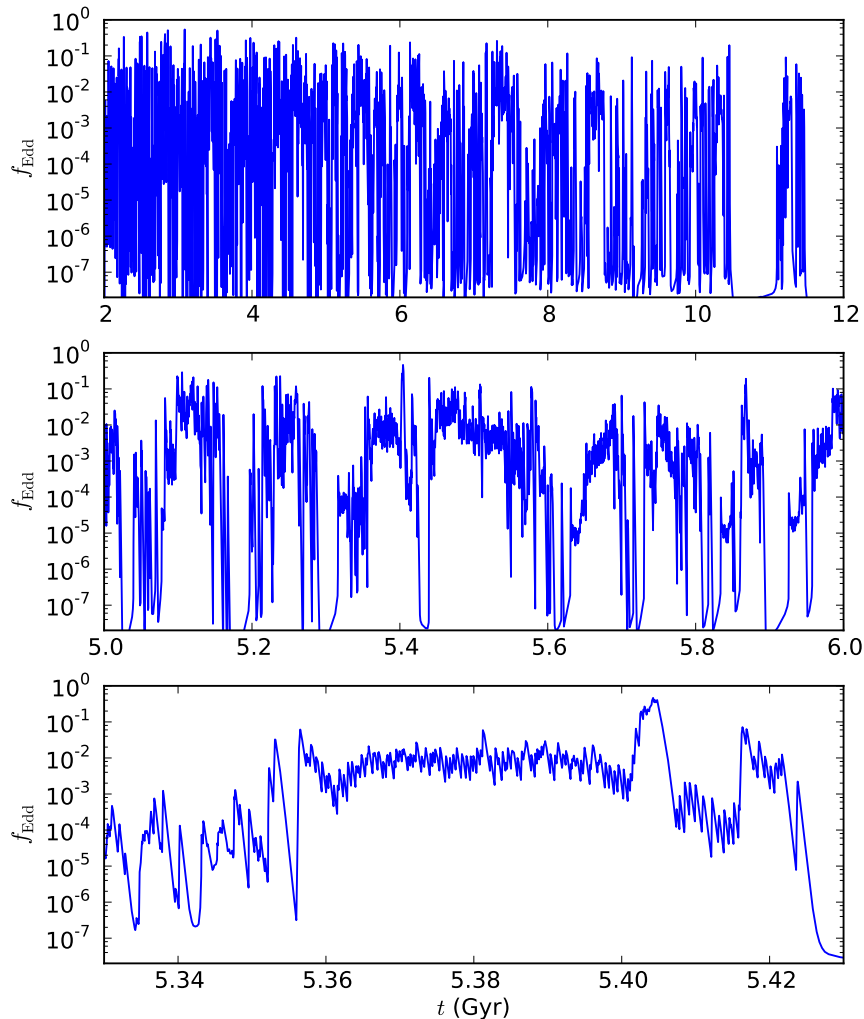


FIG. 6.— Eddington ratio as a function of time, for three different time intervals in the *A2* simulation.

3.4. Star Formation and Galactic Winds, and Gas Content

Table 1 gives total mass of stars formed, total mass of gas driven beyond $10R_e$, and final mass of gas within $10R_e$ for each simulation. Star formation consumes about 30% of the total mass budget in the two-dimensional simulations and is very insensitive to the details of the AGN feedback. This is in good agreement with the one-dimensional simulations at low mechanical efficiencies. However, at high feedback efficiencies, the one-dimensional simulations drive significant quantities of gas out of the galaxy, leading to low star formation rates and low final gas content. In this respect the one-dimensional and two-dimensional simulations disagree. However, this is to be expected since assuming spherical symmetry gives the most favorable situation for turning a central energy source into a global outflow. In two dimensions, energy can escape via low-density channels and fail to participate in driving an outflow.

Figure 10 shows the mean mechanical energy input versus the mean efficiency for one-dimensional and two-dimensional A models. For two-dimensional A models, the energy input is nearly constant—the SMBH accretion self-regulates to provide energy at this rate. The one-dimensional A models have lower energy input rates. That is, two-dimensional models require more energy to reach equilibrium between inflow (due to cooling) and outflow (due to mechanical feedback).

4. CONCLUSIONS

We have performed two-dimensional simulations of the entire cosmic history (12 Gyr) of an isolated L_* elliptical galaxy. Planetary nebulae and red giant winds produced by evolving low-mass stars serve as the source of gas in the galaxy. This gas finally ends up either in the central BH, in long-lived low-mass stars (formed in the simulation), in the ISM within the galaxy (at the end of the simulation), or outside the galaxy as part of the intergalactic medium. As gas finds its way to one of those four

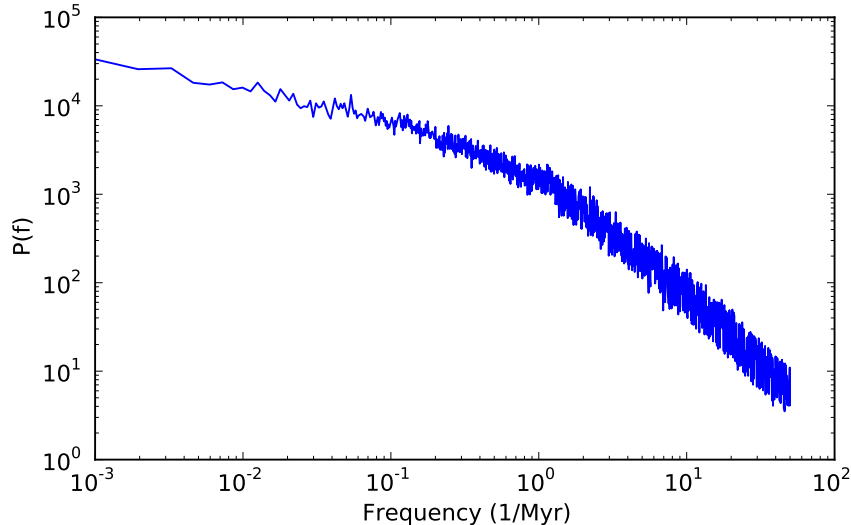


FIG. 7.— Power spectrum of the dimensionless mass accretion rate $\dot{M}_{\text{BH}}/\dot{M}_{\text{Edd}}$ for A2. The units of the y -axis are arbitrary. For frequencies higher than the inverse of several times the central accretion disk timescale, the power spectrum is proportional to $1/f$, the frequency response of the low-pass filter applied by our central accretion disk. For lower frequencies, the power spectra are determined by the physics of gas input, cooling, and feedback. At these low frequencies, the power spectrum is nearly flat: $\propto f^{-1/4}$. That is, the accretion onto the SMBH has a power spectrum nearly the same as white noise.

TABLE 1
PROPERTIES OF COMPUTED MODELS

Model	ϵ_W	$\langle\epsilon_{\text{EM}}\rangle$	$\log \Delta M_{\text{BH}}$	$\log \Delta M_*$	$\log \Delta M_W$	$\log M_{\text{gas}}$
A0	5×10^{-3}	0.041	7.40	9.98	10.28	9.67
A05	10^{-3}	0.060	8.10	9.94	10.33	9.50
A1	2.5×10^{-4}	0.067	8.71	9.88	10.35	9.45
A2	10^{-4}	0.067	9.18	9.91	10.29	9.49
A3	5×10^{-5}	0.063	9.55	9.94	10.17	9.58
A4	3×10^{-5}	0.060	9.72	9.93	10.11	9.50
A5	1×10^{-5}	0.048	9.71	9.98	10.03	9.50
A6	3×10^{-6}	0.047	9.69	10.00	10.03	9.52
A7	1×10^{-6}	0.047	9.69	9.99	10.03	9.52

NOTE. — Final properties of the simulated galaxies, where ϵ_W is the mechanical wind efficiency, $\langle\epsilon_{\text{EM}}\rangle$ is the mass-weighted mean radiative efficiency, ΔM_{BH} is the change in the mass of the BH, ΔM_* is the mass of stars formed during the simulation, ΔM_W is the total gas mass driven beyond 10 effective radii, and $\log M_{\text{gas}}$ is the total mass remaining within 10 effective radii.

final states, it can engage in star formation, mass/energy injection into the ISM via Type Ia or Type II supernovae, or radiative cooling.

The primary purpose of the code is to implement the well-developed physical model of mechanical and radiative AGN feedback of Ciotti et al. (2009b). This model includes momentum and energy imparted to the gas by Compton scattering and atomic lines via radiation from the central SMBH. It also includes a self-consistent model of mechanical feedback via a broad-line wind. The primary difference between the two-dimensional code and the one-dimensional code (upon which it is based) is that the two-dimensional code does not yet include the physics of optically thick radiation pressure on dust grains. Experiments with the one-dimensional code have shown that turning off the dust opacity does not greatly affect the SMBH growth, although other aspects of the simulation results such as the star formation rate are affected.

Multi-dimensional simulations are a significant improvement over the one-dimensional simulations because the additional degrees of freedom allow classical instabilities such as the RT or Kelvin–Helmholtz instabilities to operate. The RT instability in particular plays an important role because AGN feedback tends to produce a hot bubble of gas near the SMBH, effectively halting accretion. In one dimension, the bubble cannot move away from the SMBH and continues to suppress subsequent infall until it itself radiatively cools. In two dimensions, the hot bubble buoyantly moves up through the ISM and additional cold gas generated at radii of 0.1–1 kpc can freely fall into the center of the simulation.

In this work, we have assumed a low specific angular momentum profile for the model galaxy in order to match the one-dimensional simulations as closely as possible. The effect of angular momentum transport in galaxies with more typical specific angular momenta is likely to

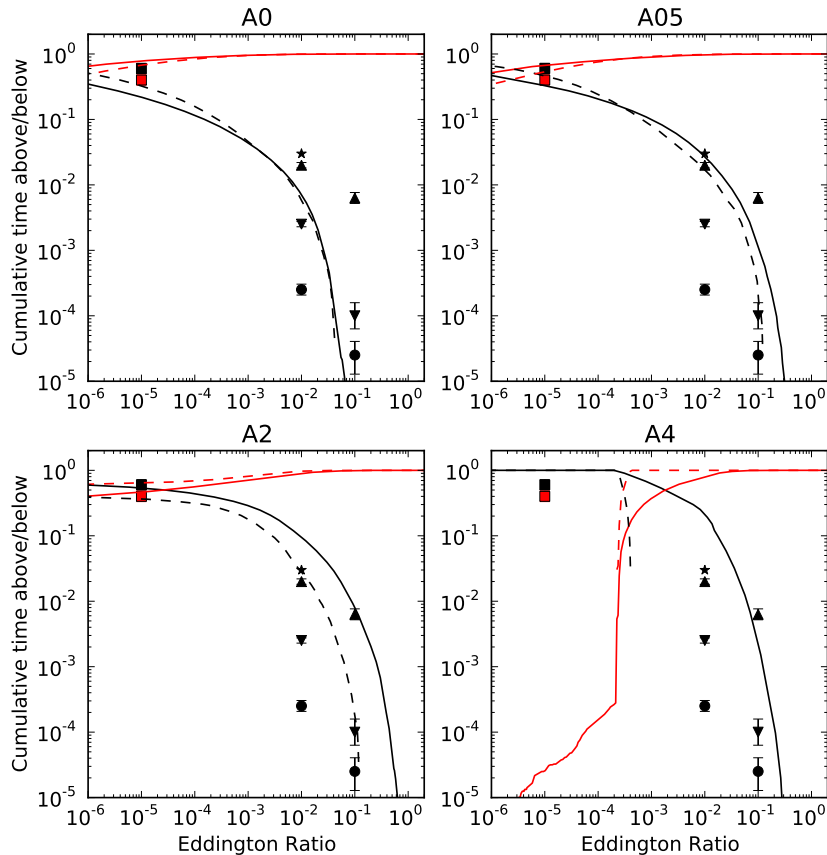


FIG. 8.— AGN duty cycle as a function of Eddington ratio for the A2 simulation. The black/red lines show the cumulative time above/below the given Eddington ratio. Solid lines are computed using the entire simulation time, while dashed lines use only the final 2 Gyr. Points are observational constraints and are similarly colored black or red according to whether they are measurements of the fraction of objects above or below the given Eddington ratio. Downward-pointing triangles are from Heckman et al. (2004), circles from Greene & Ho (2007), upward-pointing triangles from Kauffmann & Heckman (2009), and squares are from Ho (2009). All of these use low-redshift observations and should thus be compared to the dashed lines. The star is a constraint from Steidel et al. (2003) for the Lyman-break galaxies at high redshift showing nuclear activity, and therefore should be compared to the solid lines. There is significant observational disagreement about the fraction of $3 \times 10^8 M_{\odot}$ BHs accreting at 1% or 10% of the Eddington rate, even at low redshift. Nevertheless, the A05 and A2 simulations fit both the high-redshift and low-redshift constraints reasonably well given the state of the observational data.

be very important. We plan to implement angular momentum transport in future work in order to isolate its affect on our results.

An important feature of our simulations is that we have taken care to resolve the Bondi radius even for gas heated to the Compton temperature by the AGN. The gas heating terms due to AGN radiation go as $1/r^2$, becoming much more effective as a given parcel of gas moves toward the BH. If the Bondi radius is resolved even for the hot gas, then our conclusion about whether or not a given parcel of gas makes it to the center of the simulation is secure. If the Bondi radius is not resolved, then radiative heating that would have occurred between the inner radius of the simulation and the physical Bondi radius might have increased the temperature of the gas to the point that thermal energy dominated over gravitational energy—the gas would not make it to the SMBH. Thus if the Bondi radius is not resolved for the hot as well as the cold gas, we cannot be sure whether or not a given parcel of gas actually makes it to the SMBH.

Resolving the Bondi radius for the hot gas requires high

central spatial resolution. The large velocities of the BAL wind entering the grid near the center necessitate time steps of order one year. The timescale relevant for stellar evolution, the physical source of the gas, is several Gyr. We have opted to use rather coarse spatial resolution in order to run the simulations long enough to see evolution over the entire cosmic history of the galaxy in question.

The primary differences between the previously presented one-dimensional simulations and the present two-dimensional simulations are that the character of the accretion as a function of time changes from well-separated, dramatic bursts (one dimension) to chaotic, stochastic accretion (two dimensions). There are two reasons for this. First, the cold, infalling gas generated at a few hundred parsecs tends to fragment and fall into the SMBH as several discrete blobs (two dimensions) rather than as a coherent spherical shell (one dimension). Second, the RT instability allows hot gas generated via radiative heating by the AGN to move out of the way, allowing subsequent blobs of cold gas to fall into the SMBH unimpeded. Thus, a burst of accretion in two dimensions is much less effec-

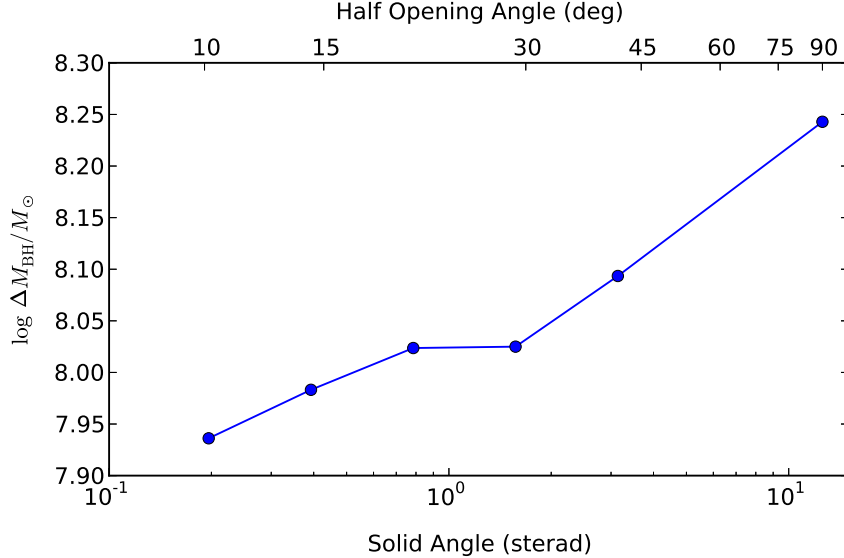


FIG. 9.— Change in SMBH mass vs. wind opening angle for $\epsilon_W = 10^{-3}$. Mechanical feedback becomes less effective for opening angles larger than 45° , corresponding to a covering fraction of 1/4 of the sky. Overall, the change in BH growth is less than a factor of two for a wide range of wind opening angles.

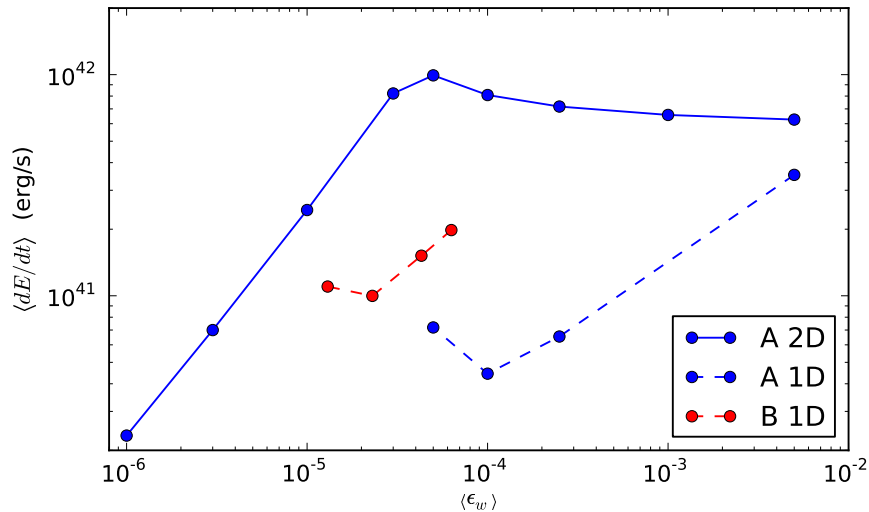


FIG. 10.— Time-averaged mean energy input ($\int \dot{E} dt / \int dt$) via AGN mechanical feedback vs. mass-averaged mean feedback efficiency ($\int \epsilon \dot{m} dt / \int \dot{m} dt$). For the two-dimensional simulations, at the low-efficiency end, energy input falls off because the SMBH is consuming all of the mass available to it: ΔM_{BH} is at a maximum but ϵ_W is still falling. At the high-efficiency end, energy input approaches a constant—the simulation self-regulates to an energy input of $\simeq 5 \times 10^{41}$ erg s $^{-1}$. This implies a nearly perfect, inverse relationship between ΔM_{BH} and ϵ_W at the high-efficiency end. The one-dimensional simulations have smaller energy inputs at a given efficiency, reflecting their smaller SMBH growth rates.

tive at stopping subsequent accretion than is the case in one dimension.

Another way of saying this is that mechanical feedback is less effective in two dimensions than one dimension: it takes more energy for a given galaxy model to reach equilibrium between cooling-driven inflow and feedback-driven outflow/heating. At a fixed mechanical efficiency, the SMBH self-regulates to larger mean accretion rates in order to provide the required additional energy.

Two-dimensional outflows are less effective than spherical ones in two critical aspects. less effective in protecting the SMBH from infalling gas and less effective in

ejecting gas from the galaxy.

For our models with wind efficiencies of 10^{-3} and 10^{-4} , the distribution of Eddington ratios is in reasonable agreement with the observed fraction of galaxies above/below a given Eddington ratio over four orders of magnitude in luminosity. These values of the efficiency are both physically plausible and supported by recent observations (Arav et al. 2011).

Our plans for future work include implementing optically thick radiative transfer on dust to bring the physics of our treatment of AGN and star-formation feedback up to the state of the art. Furthermore, the B models for

mechanical feedback are more realistic in the sense that the efficiency and opening angle both become small at low accretion rates, in line with observational and theoretical expectations. The one-dimensional simulations produced B models in good agreement with observations (Ciotti et al. 2010), but using identical parameters for two-dimensional simulations did not result in the same good agreement. A parameter study of B models in two dimensions is necessary to identify viable ranges of the parameters. Finally, there remain many potentially important physical processes that we have not attempted to model in this work—energy transport via conduction and the extent to which conduction is suppressed by tangled magnetic fields among them.

In this paper, we have focused on the comparison between one-dimensional and two-dimensional AGN feedback models with nearly the same implemented physics and spatial resolution. A future study will put this

model into better context by comparing more thoroughly to the existing AGN feedback models in the literature (e.g., Di Matteo et al. 2005; Johansson et al. 2009; Debuhr et al. 2010).

ACKNOWLEDGMENTS

We thank Jenny Greene, Jim Stone, and Daniel Proga for useful discussions, Nahum Arav for making results available in advance of publication, and the anonymous referee for a very thoughtful and helpful report. G.S.N. was supported by the Princeton University Council on Science and Technology and grants NASA NNX08AH31G and NAS8-03060. G.S.N. also made extensive use of the computing facilities of the Princeton Institute for Computational Science and Engineering. J.P.O. acknowledges the support of NSF grant AST-0707505. L.C. was supported by the MIUR grant PRIN2008.

REFERENCES

- Alvarez, M. A., Wise, J. H., & Abel, T. 2009, *ApJ*, 701, L133
 Arav, N., Dunn, J. P., Korista, K., Edmonds, D., González-Serrano, J. I., Benn, C., & Jiménez-Luján, F. 2011, *ApJ*, submitted
 Arieli, Y., Rephaeli, Y., & Norman, M. L. 2010, *ApJ*, 716, 918
 Ciotti, L., Morganti, L., & de Zeeuw, P. T. 2009a, *MNRAS*, 393, 491
 Ciotti, L., & Ostriker, J. P. 1997, *ApJ*, 487, L105
 —. 2001, *ApJ*, 551, 131
 —. 2007, *ApJ*, 665, 1038
 Ciotti, L., Ostriker, J. P., & Proga, D. 2009b, *ApJ*, 699, 89
 —. 2010, *ApJ*, 717, 708
 Croton, D. J., et al. 2006, *MNRAS*, 365, 11
 Debuhr, J., Quataert, E., Ma, C., & Hopkins, P. 2010, *MNRAS*, 406, L55
 Debuhr, J., Quataert, E., & Ma, C.-P. 2011, *MNRAS*, 412, 1341
 Di Matteo, T., Springel, V., & Hernquist, L. 2005, *Nature*, 433, 604
 Djorgovski, S., & Davis, M. 1987, *ApJ*, 313, 59
 Dressler, A., Lynden-Bell, D., Burstein, D., Davies, R. L., Faber, S. M., Terlevich, R., & Wegner, G. 1987, *ApJ*, 313, 42
 Emsellem, E., et al. 2007, *MNRAS*, 379, 401
 —. 2004, *MNRAS*, 352, 721
 Faber, S. M., & Jackson, R. E. 1976, *ApJ*, 204, 668
 Fabian, A. C., Vasudevan, R. V., Mushotzky, R. F., Winter, L. M., & Reynolds, C. S. 2009, *MNRAS*, 394, L89
 Ferrarese, L., & Merritt, D. 2000, *ApJ*, 539, L9
 Field, G. B. 1965, *ApJ*, 142, 531
 Gavazzi, R., Treu, T., Koopmans, L. V. E., Bolton, A. S., Moustakas, L. A., Bures, S., & Marshall, P. J. 2008, *ApJ*, 677, 1046
 Gavazzi, R., Treu, T., Rhodes, J. D., Koopmans, L. V. E., Bolton, A. S., Bures, S., Massey, R. J., & Moustakas, L. A. 2007, *ApJ*, 667, 176
 Gebhardt, K., et al. 2000, *ApJ*, 539, L13
 Greene, J. E., & Ho, L. C. 2007, *ApJ*, 667, 131
 Gültekin, K., et al. 2009, *ApJ*, 698, 198
 Heckman, T. M., Kauffmann, G., Brinchmann, J., Charlot, S., Tremonti, C., & White, S. D. M. 2004, *ApJ*, 613, 109
 Ho, L. C. 2009, *ApJ*, 699, 626
 Hopkins, P. F., & Quataert, E. 2010a, arXiv:1007.2647
 —. 2010b, *MNRAS*, 407, 1529
 Johansson, P. H., Naab, T., & Burkert, A. 2009, *ApJ*, 690, 802
 Kauffmann, G., & Heckman, T. M. 2009, *MNRAS*, 397, 135
 Kurosawa, R., & Proga, D. 2009a, *MNRAS*, 397, 1791
 —. 2009b, *ApJ*, 693, 1929
 Kurosawa, R., Proga, D., & Nagamine, K. 2009, *ApJ*, 707, 823
 Levine, R., Gnedin, N. Y., Hamilton, A. J. S., & Kravtsov, A. V. 2008, *ApJ*, 678, 154
 Magorrian, J., et al. 1998, *AJ*, 115, 2285
 Metzler, C. A., & Evrard, A. E. 1994, *ApJ*, 437, 564
 Narayan, R., & Yi, I. 1994, *ApJ*, 428, L13
 Novak, G. S., Faber, S. M., & Dekel, A. 2006, *ApJ*, 637, 96
 Omma, H., & Binney, J. 2004, *MNRAS*, 350, L13
 Ostriker, J. P., Choi, E., Ciotti, L., Novak, G. S., & Proga, D. 2010, *ApJ*, 722, 642
 Park, K., & Ricotti, M. 2010, arXiv:1006.1302
 Proga, D., Stone, J. M., & Kallman, T. R. 2000, *ApJ*, 543, 686
 Reeves, J. N., et al. 2009, *ApJ*, 701, 493
 Sazonov, S. Y., Ostriker, J. P., Ciotti, L., & Sunyaev, R. A. 2005, *MNRAS*, 358, 168
 Shakura, N. I., & Sunyaev, R. A. 1973, *A&A*, 24, 337
 Shin, M., Ostriker, J. P., & Ciotti, L. 2010, *ApJ*, 711, 268
 Sijacki, D., Springel, V., Di Matteo, T., & Hernquist, L. 2007, *MNRAS*, 380, 877
 Soltan, A. 1982, *MNRAS*, 200, 115
 Springel, V., Di Matteo, T., & Hernquist, L. 2005, *ApJ*, 620, L79
 Steidel, C. C., Adelberger, K. L., Shapley, A. E., Pettini, M., Dickinson, M., & Giavalisco, M. 2003, *ApJ*, 592, 728
 Sternberg, A., & Soker, N. 2008, *MNRAS*, 384, 1327
 Stone, J. M., & Norman, M. L. 1992, *ApJS*, 80, 753
 Tremaine, S., et al. 2002, *ApJ*, 574, 740